ACS OMEGA

http://pubs.acs.org/journal/acsodf

Article

Effects of Pellet Basicity on the Simulated Deposit Formation in Coal-Fired Rotary Kilns for Iron Ore Pellet Production

Yufeng Guo, Zhuang Yang, Jianjun Fan, Shuai Wang,* Feng Chen, Lingzhi Yang, Yajing Liu, and Kuo Liu

Cite This: *ACS Omega* 2022, 7, 4640−4647

Read Online

ACCESS | Metrics & More | Article Recommendations

ABSTRACT: Deposit formation in the coal-fired rotary kiln is frequently found in the production of fluxed iron ore pellets by the grate-kiln process and affects normal production. In this paper, the effects of pellet basicity (CaO/SiO_2 mass ratio) on the simulated deposit formation were investigated. The results show that the porosity of deposits samples increases from 30.8 to 41.5% as the pellet basicity increases from 0.6 to 1.2, and most of the holes are irregular in shape. The contents of CaO and Fe_2O_3 in the silicates of the deposit samples increased with increasing basicity. The primary phase of the deposit samples changed from the M_2O_3 phase region to the clinopyroxene phase region with a lower melting point. As the basicity increased, the calculated proportions of the liquid phases in the deposit samples had an increasing trend. Moreover, the deposit sample adhesion to the refractory brick increases with the increase in pellet basicity.

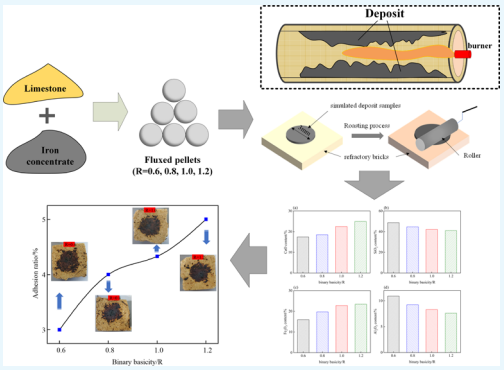

1. INTRODUCTION

Iron ore pellets are an essential part of the blast furnace charge, with high grade, good strength, uniform particle size, good metallurgical properties, and so forth.[1,2] Especially, fluxed iron ore pellets have better high-temperature soft fusion performance and reduction performance.[3−5] However, the burden of the blast furnace is still dominated by a high proportion of high basicity sinter and some acidic iron ore pellets.[1] The pelletizing process's energy consumption, CO_2 emission, and environmental pollution are much lower than the sintering process. In order to optimize the structure of the blast furnace burden and reduce the environmental pollution,[6] some companies have focused on the production of fluxed iron ore pellets to replace the iron ore sinter for blast furnace smelting in recent years.[7]

The three common processes used in iron ore pellet production are the shaft furnace process, the straight grate process, and the grate-kiln process.[8] As the dominant process for iron ore pellet production in China, the proportion of iron ore pellets produced by the grate-kiln process has exceeded 70%.[9] Deposit formation in a rotary kiln is frequently observed in iron ore pellet production by the grate-kiln process, disturbing normal production and decreasing productivity.[10] The deposit of fluxed iron ore pellets is more severe than acidic iron ore pellet production.[11,12]

Many researchers[13−19] have focused on the deposition mechanism in rotary kilns for acidic iron ore pellet productions. In the rotary kilns fueled by pulverized coal, preheated iron ore pellet powder and coal ash are the material basis for deposit formation. The characterization of the deposits showed that the main mineralogical phases include hematite, silicate, and some minor glass phases.[20−23] Some studies have found differences in the mechanism of deposit formation in different parts of the rotary kiln.[13,24] The primary manner to form the deposits near the burner zone in the rotary kiln was the hematite crystallization and diffusion, while the liquid phases played a secondary role in the deposit formation. Furthermore, bentonite and coal ash contain high SiO_2, Al_2O_3, Na_2O, and K_2O, which will promote the generation of liquid phases and intensify the deposition phenomenon.[17,25,26] In addition, insufficient combustion of pulverized coal caused partial zones of the reduction atmosphere in the rotary kiln, resulting in the generation of Fe^{2+}, and formed low-melting-temperature compounds with veinstone minerals such as SiO_2 and CaO Al_2O_3.[27−29] It has been found that the deposition phenomenon became more severe in rotary kilns for producing fluxed iron ore pellets.[30,31] Unfortunately, the effects of the basicity of iron ore pellets on the deposition formation mechanism are still not fully understood. Thus, it is necessary to study the deposit formation mechanism during the production of fluxed iron ore pellets by the grate-kiln process.

During coal-fired iron ore pellet production, the deposits formed in the rotary kiln originate from the fragmentized pellet

Received: December 1, 2021
Accepted: January 17, 2022
Published: January 26, 2022

https://doi.org/10.1021/acsomega.1c06800
ACS Omega 2022, 7, 4640−4647

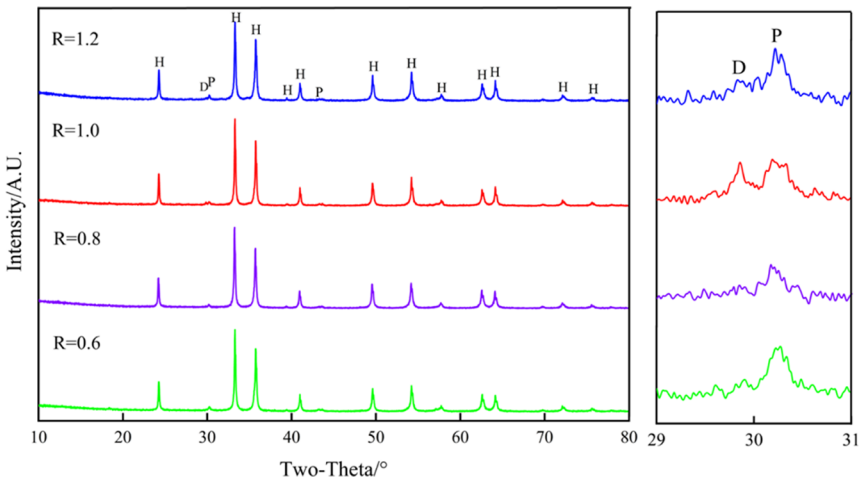

Figure 1. XRD patterns of simulated deposit samples with pellet basicity of 0.6, 0.8, 1.0, and 1.2: hematite (H), pyroxene (P), and diopside subsilic ferrian (D).

and coal ash. The generated liquid phases in the deposits are critical for the adhesion and growth of the deposits on the surface of refractory bricks. The higher proportion of liquid phases in the system would accelerate the deposit formation. Thus, this study prepared the simulated deposit samples with different basicity by mixing preheating pellets powder and coal ash. The effects of the basicity of iron ore pellets on the microstructure, phase composition, and elemental distribution behaviors of the deposits are investigated. Moreover, the phase diagram and liquid phase generation of the bonded phase were calculated by FactSage 8.0 software. Finally, the effects of basicity on adhesivity of simulated deposits to refractory were presented. Our study will provide a technical basis for understanding the effects of binary basicity of iron ore pellets on deposition formation and guiding the fluxed iron pellet production in China.

2. RESULTS AND DISCUSSION

2.1. Phase Compositions of the Roasted Deposit Samples. The X-ray diffraction (XRD) analysis of each binary basicity simulated deposition sample is shown in Figure 1. The main material phase of the simulated deposition is hematite, and minor silicate phases are pyroxene and diopside subsilic ferrian. A large amount of SiO_2, Al_2O_3, and other minerals in coal ash mixed into the iron ore pellet powder, which prompted the formation of silicates. In general, the silicates such as pyroxene and diopside have low softening temperatures and melting temperatures and form more liquid phases in the deposits.

2.2. Microstructure of the Roasted Deposit Samples. Figure 2 shows the microstructure of the roasted deposit samples with different binary basicity. The effects of binary basicity on the porosity of roasted deposited samples were analyzed by Image J software. The porosity of deposit samples increases from 30.8 to 41.5% as the pellet basicity increases from 0.6 to 1.2, and most of the holes are irregular in shape. In particular, when the binary basicity reaches 1.2, the roasted deposit samples appear to have significant cracks. At high temperatures, the silicate phase in the deposited sample generates liquid phases to bond the solid phase and shrink in volume. At the same time, the higher binary basicity needs more limestone addition. The limestone starts to decompose (about 759 °C) to produce CO_2, leading to the generation of holes in the roasted sample. The burning of residual carbon in deposit samples may also cause holes in the roasted samples.

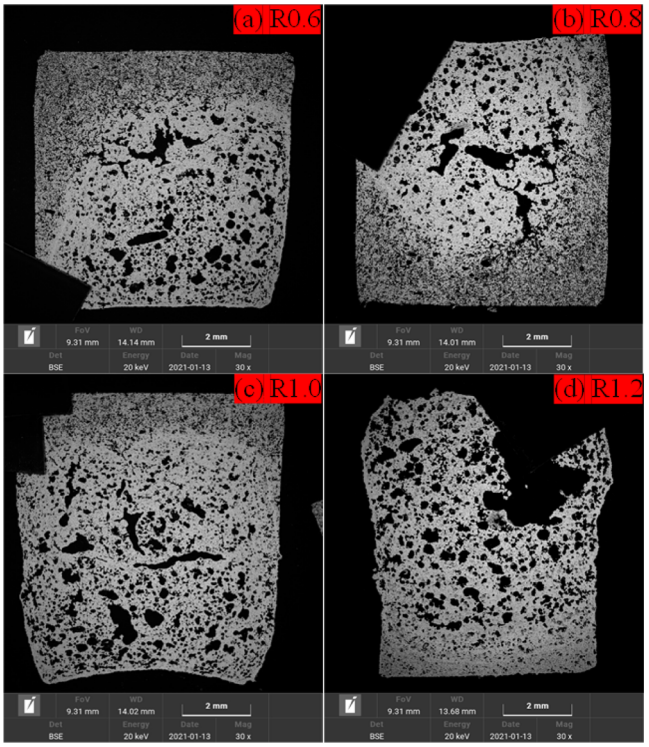

Figure 2. Microstructure of the roasted deposit samples with different binary basicity: (a) R = 0.6, (b) R = 0.8, (c) R = 1.0, and (d) R = 1.2.

2.3. Elemental Distributions of the Roasted Deposit Samples. The microstructure and elemental distribution of the roasted deposit samples are also shown in Figures 3−6. It is evident that when the binary basicity is 0.6 and 0.8, hematite particles are mainly bonded in the recrystallized solid phase, and the hematite particles are uneven. When the binary basicity is further increased to 1.0 and 1.2, the deposited samples probably generate higher proportions of liquid phases, which play an essential role in the growth of the deposition.

Figure 3 shows the energy-dispersive spectrometry (EDS) analysis of the deposit sample with a binary basicity of 0.6, and the main elemental composition of the deposit bonding phase is

https://doi.org/10.1021/acsomega.1c06800
ACS Omega 2022, 7, 4640−4647

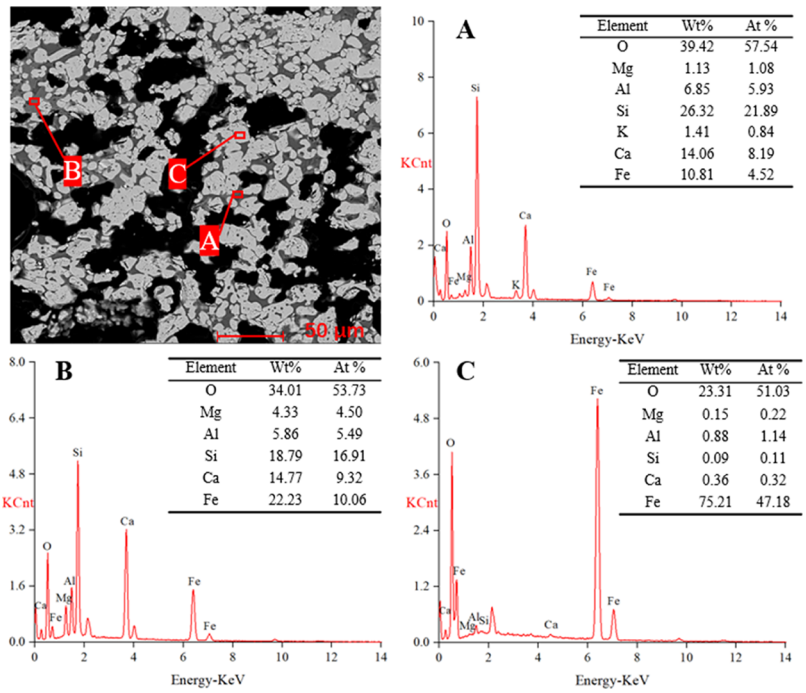

Figure 3. EDS analysis of simulated deposited samples with a binary basicity of 0.6: (A) EDS results of silicate with low iron, (B) EDS results of silicate with high iron, and (C) EDS results of hematite.

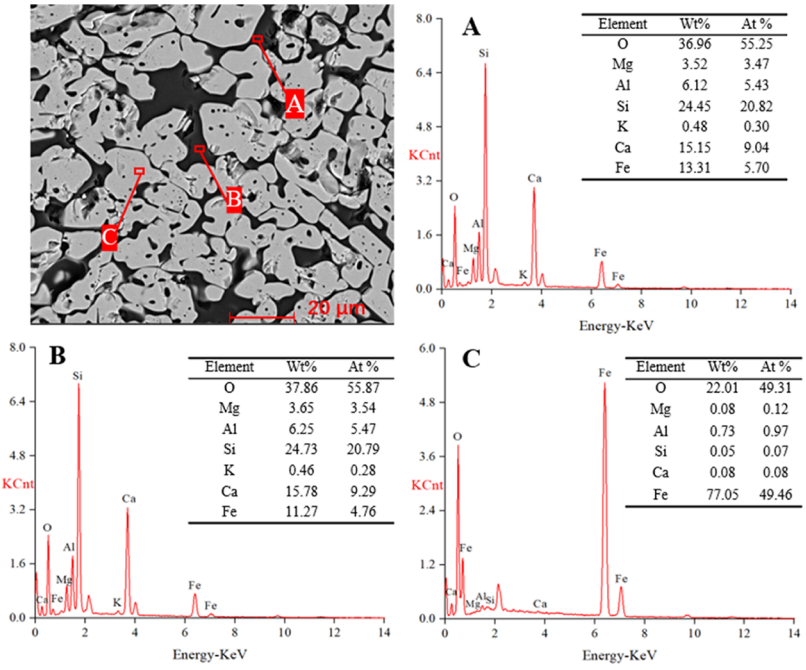

Figure 4. EDS analysis of simulated deposited samples with a binary basicity of 0.8: (A) EDS results of silicate A, (B) EDS results of silicate B, and (C) EDS results of hematite.

O, Si, and Ca and a minor amount of Al, Mg, Fe, and K. The bonding phases are mainly silicate phase with high iron content (point B) and silicate phase with low iron content and high silica content (point A).

Figures 4−6 show that the deposits are composed of a hematite phase with a dark gray silicate phase. The chemical compositions of the silicates vary as the binary basicity increases. More Ca ions are introduced into the silicate phase. The Ca content of silicates with low iron (point A) increases from 14.06 to 23.43 wt %, and the Ca content of silicates with high iron (point B) increases from 14.77 to 16.41 wt % as the pellet basicity increase from 0.6 to 1.2.

2.4. Chemical Composition of Bonding Phases and Liquid Phase Generation. It can be inferred that the chemical composition of silicates (bonding phase) in the deposits with different pellet basicity changed with various pellet basicity. In general, the change in the chemical composition of bonding phases would significantly influence the formation of liquid phases and deposit formation. Thus, the elemental compositions of the bonding phases with different binary basicity were

https://doi.org/10.1021/acsomega.1c06800
ACS Omega 2022, 7, 4640−4647

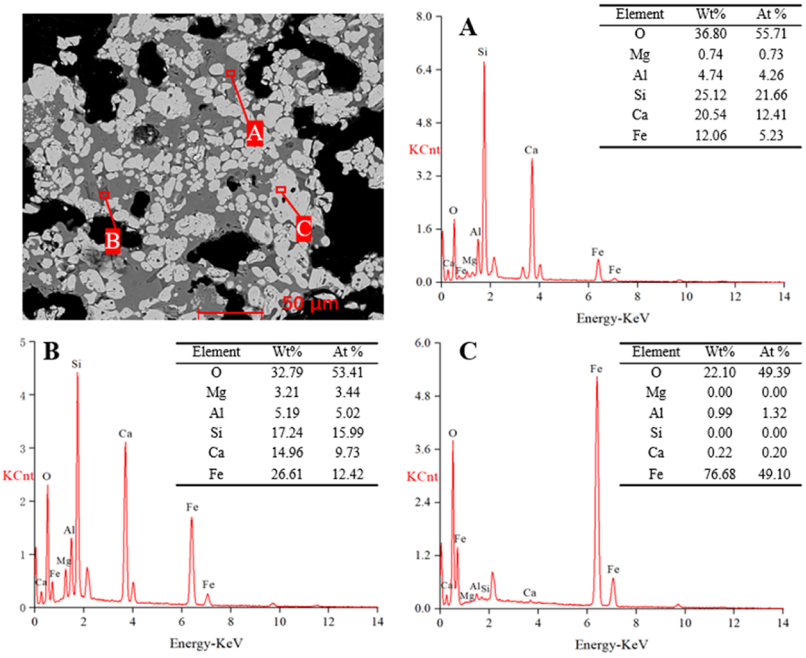

Figure 5. EDS analysis of simulated deposited samples with a binary basicity of 1.0: (A) EDS results of silicate with low iron, (B) EDS results of silicate with high iron, and (C) EDS results of hematite.

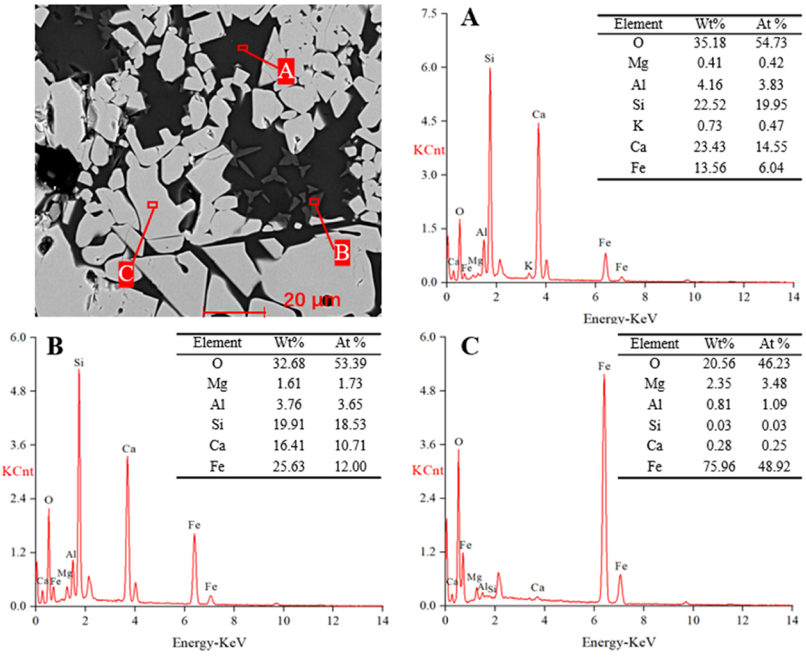

Figure 6. EDS analysis of simulated deposited samples with a binary basicity of 1.2: (A) EDS results of silicate with low iron, (B) EDS results of silicate with high iron, and (C) EDS results of hematite.

obtained by collecting the EDS results of silicates in the deposit samples. The composition of the bonding phase of the roasted deposit samples mainly includes SiO_2, CaO, Fe_2O_3, and Al_2O_3. Based on the results of EDS analysis, the average chemical compositions of the roasted deposit samples with different binary basicity were counted from at least 10 points.

As illustrated in Figure 7, it can be concluded that with the increase in binary basicity of iron ore pellets, the content of CaO and Fe_2O_3 in the bonding phase of roasted samples tends to increase, while the content of SiO_2 and Al_2O_3 tends to decrease. The CaO content in the bonding phase reached 25% by adding more limestone, while the SiO_2 content was above 40%.

The phase diagram of the SiO_2−CaO−Fe_2O_3−10% Al_2O_3−5% MgO system was drawn using FactSage 8.0[32] software to reveal the effects of composition change in bonding phases. As shown in Figure 8, for the change in the bonding phase composition from "A" to "B" for the roasted deposited samples, "A" represents the bonding phase composition of the deposited samples with an iron ore pellet binary basicity of 0.6, and "B" represents a higher binary basicity of 1.2. It can be seen that the bonding phase composition in deposited samples changes from

https://doi.org/10.1021/acsomega.1c06800
ACS Omega 2022, 7, 4640−4647

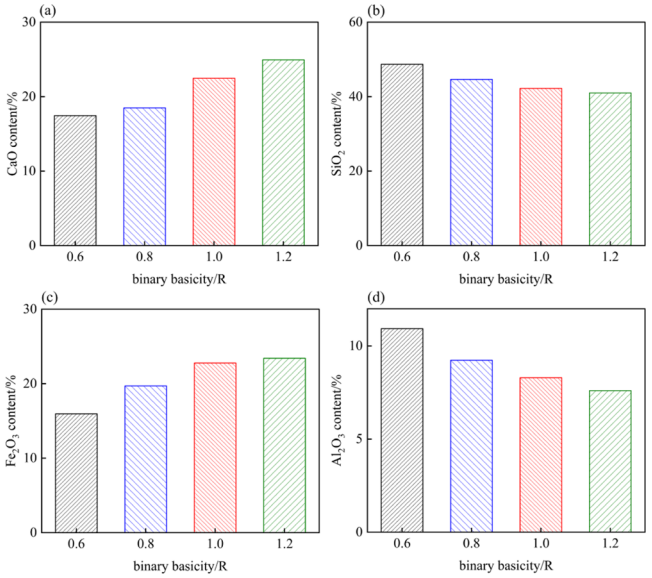

Figure 7. Effect of pellet binary basicity on the chemical composition of the bonding phase of deposit samples: (a) CaO content, (b) SiO_2 content, (c) Fe_2O_3 content, and (d) Al_2O_3 content.

the M_2O_3 phase area to the clinopyroxene phase area as the binary basicity increases. Pyroxene is a common silicate rock-forming mineral with a single-stranded structure. The crystal structure is monoclinic or orthoclinic, and monoclinic pyroxene has a low melting temperature. It forms co-crystals with quartz and Fe_2O_3 with melting temperatures below 1200 °C, promoting the liquid phase generation.

In addition, the average proportions of liquid phases of bonding phases at 1200, 1250, and 1300 °C were calculated and are shown in Figure 9. The amounts of liquid phase generation in

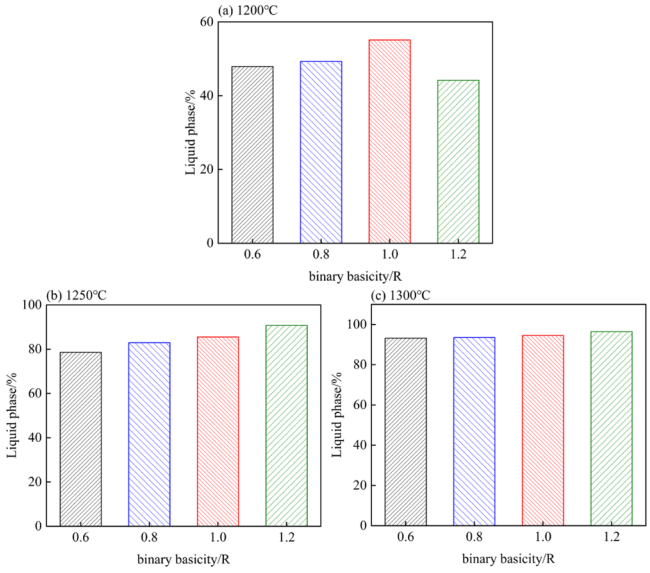

Figure 9. Effect of binary basicity on the ratio of the liquid phase of the bonding phase in deposited samples: (a)1200, (b)1250, and (c)1300 °C.

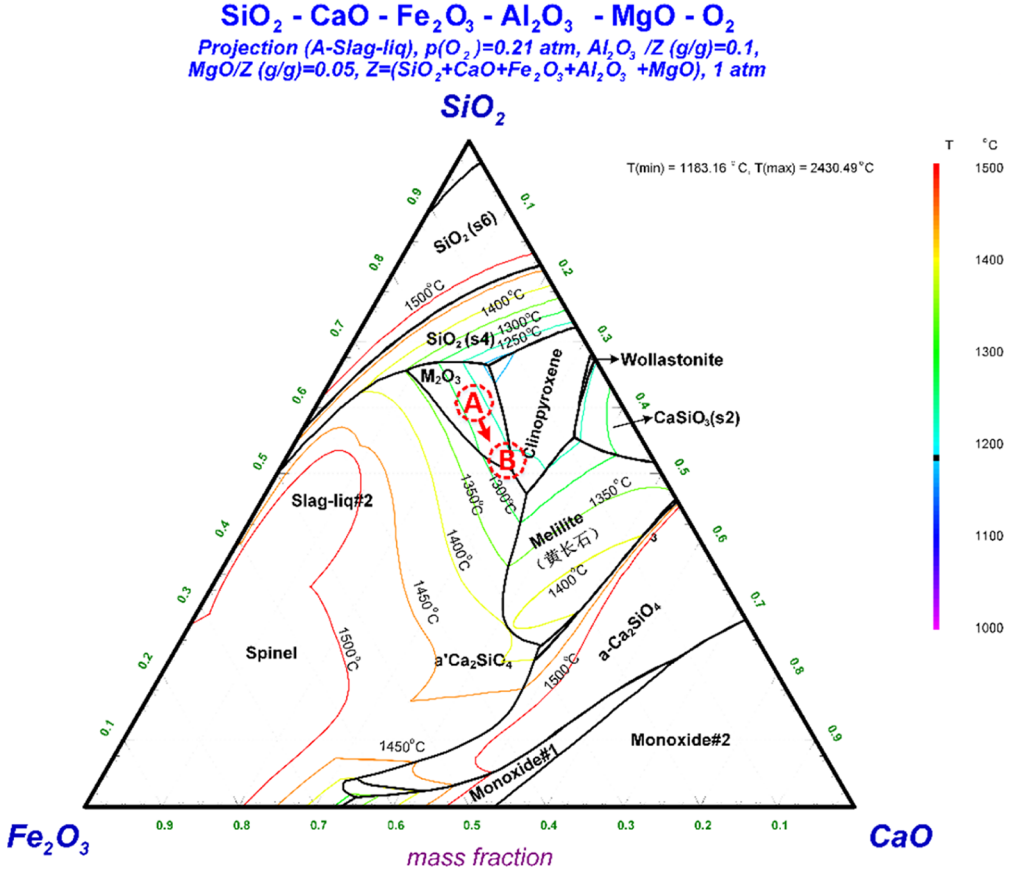

Figure 8. Phase diagram of the SiO_2−CaO−Fe_2O_3−10% Al_2O_3−5% MgO system.

https://doi.org/10.1021/acsomega.1c06800
ACS Omega 2022, 7, 4640−4647

the bonding phases have a rising trend as the binary basicity of iron ore pellets increases. This can be explained by the fact that more CaO was added and reacted with iron oxides to produce calcium ferrate silicates with a lower melting temperature, generating more liquid phases.

The calculation results show that the average liquid phase generation of the bonding phase for samples with the binary basicity of 0.6 and 1.2 is about 45% at 1200 °C, while the binary basicity of 0.8 and 1.0 is above 50%. When the roasting temperature was 1250 °C, the liquid phase generation of the bonding phase of the sample with a binary basicity of 1.2 was already more than 90%. In addition, when the temperature is further increased to 1300 °C, the liquid phase generation capacity reaches a very high level. In producing high basicity pellets by the grate-kiln process, deposit formation is greatly influenced by the kiln temperature. The thermal regime should be strictly controlled to reduce temperature fluctuations and local overheating in the kiln.

2.5. Effect of Binary Basicity on the Adhesion of Deposits on Refractory Bricks. Deposits in a rotary kiln result from powder continuously bonded to the kiln refractories at high temperatures; the formation process is long and about several months. The adhesion rate of deposits with various basicity on the refractories was evaluated. As shown in Figure 10,

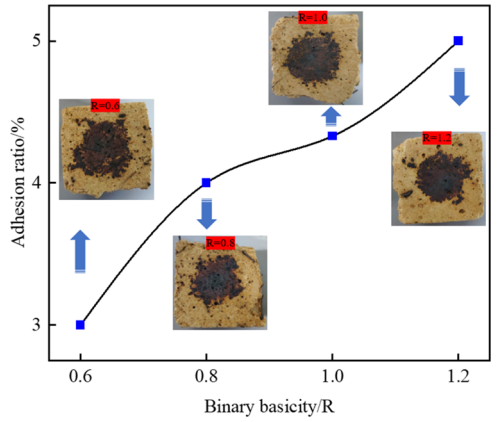

Figure 10. Deposition adhesion of different binary basicity powders on refractory bricks.

the amount of powder adherence on the refractory bricks increases as the binary basicity increases. The adhesion rate of deposit on the brick surface increases from 3.0 to 5.0%. In addition, the appearance of the refractory bricks after roasting shows that the color of the contact surface of the refractory brick become dark, which indicates that the powder interacts with the refractory brick at high temperatures and partially erodes into the refractory brick.

In summary, when the binary basicity of iron ore pellets was increased, the Ca and Fe content in bonding phases of the simulated deposits tended to increase, which further reduces its melting temperature, makes the generation of the liquid phase easier, and increases the adhesion of the pellet powder on the refractory brick. Some suggesting measures, such as adding MgO, optimizing the preheating and roasting principles, increasing the preheating pellets' strength to reduce the pellet powder, may be taken to inhibit the deposit formation in the fluxed pellet production.

3. CONCLUSIONS

This study investigated the effects of pellet basicity on the simulated deposit formation mechanism in the kiln. The chemical composition of the deposited samples is mainly hematite, with minor silicates. The microstructure of the roasted samples becomes more porous with increasing binary basicity. Moreover, the chemical composition of bonding phases of the simulated deposit samples varied with basicity of various pellets. With the increase in binary basicity, more Ca ions and Fe ions are diffused into the silicate phase. The bonded phase composition moved to the clinopyroxene phase region in the phase diagram. The melting temperature of the silicate phase decreased, which promoted the formation of the liquid phase. The amount of liquid phase generation in the bonding phase has a rising trend as the binary basicity of iron ore pellets increases. Adhesion experiments show that the deposited samples with high binary basicity were easier to adhere on refractory bricks in the rotary kiln. Some suggested measures may inhibit the deposit formation in the fluxed pellet production, including adding MgO, optimizing the preheating and roasting principles, and increasing the preheating pellets' strength to reduce the pellet powder.

4. MATERIALS AND METHODS

4.1. Materials. The raw materials used in this study were provided by an iron ore pellet plant in China and included preheated pellet, deposit sample, iron ore concentrate, limestone, bentonite, coal ash, and refractory bricks, whose chemical compositions are shown in Tables 1 and 2. Table 1 shows that

Table 2. Chemical Compositions of Refractory Bricks (wt %)

TFe	SiO_2	CaO	Al_2O_3	MgO	TiO_2
1.23	16.98	1.75	71.26	0.24	1.89

the iron ore concentrate is mainly hematite with a small amount of magnetite; its total iron grade is 64.72%. Due to the addition of bentonite and limestone, the total iron content of the preheated pellet was reduced to 62.10%, and the CaO content was increased to 4.20%. In addition, coal ash contains a large amount of SiO_2 and Al_2O_3 and 1.22% K_2O and 0.75% Na_2O,

Table 1. Chemical Compositions of the Raw Materials (wt %)

raw material	TFe	FeO	SiO_2	CaO	Al_2O_3	MgO	K_2O	Na_2O	S
preheated pellet	62.10		4.35	4.20	1.32	0.81	0.086	0.079	0.038
deposit sample	59.74	0.76	6.67	2.98	2.93	0.69	0.24	0.17	0.024
iron ore concentrate	64.72	9.90	3.75	0.46	1.11	0.76	0.07	0.06	0.04
limestone	0.52	0.14	2.32	51.82	0.46	2.63	0.17	0.025	0.025
bentonite	3.09	0.20	60.01	3.73	12.52	3.00	1.40	1.80	0.015
coal ash	4.04	0.10	51.85	8.57	26.09	1.12	1.22	0.75	0.58

https://doi.org/10.1021/acsomega.1c06800
ACS Omega 2022, 7, 4640−4647

respectively. The high alumina refractory bricks were mainly composed of corundum and mullite.

4.2. Experiment Methods. *4.2.1. Preparation of Simulated Deposit Formation.* In order to obtain the deposition samples required for the simulation experiments, we need to analyze the composition of the deposition samples. Previous studies have shown that the original material of the deposits is preheated pellet powder and coal ash.[27] The proportions of preheated pellet powder and coal ash for forming deposition can be calculated based on the elemental balances of calcium, silicon, and aluminum.[28] The calculated results indicated that the deposit sample contained 94.34 wt % preheated pellet powder and 5.66 wt % coal ash. Since the pulverized coal cannot burn completely in practical production, we chose the pulverized coal with a combustion efficiency of 90% for the subsequent study.

In addition, the raw materials, including iron ore concentrate, limestone, and bentonite, were mixed thoroughly, and the green pellets with different binary basicity were prepared using a disc pelletizer. The size of the green pellets was 10−16 mm in diameter. By adding different proportions of limestone, the binary basicity of pellets was adjusted to 0.6, 0.8, 1.0, and 1.2. The green pellets were heated in a tube furnace at 1160 °C for 10 min to produce the preheated pellets. The preheated pellets were rotated in a drum to obtain preheated pellet powder for simulated deposit sample preparation. The simulated deposit samples consist of preheated pellet powder, pure coal ash (PCA), and removed volatile pulverized coal (RVC), as shown in Table 3.

Table 3. Proportions of Materials to Prepare Deposit Samples

sample no.	preheated pellet powder/g	PCA/g	RVC/g	basicity
R0.6	9.443	0.51	0.331	0.6
R0.8	9.443	0.51	0.331	0.8
R1.0	9.443	0.51	0.331	1.0
R1.2	9.443	0.51	0.331	1.2

The prepared deposit samples were pressed into cylindrical pellets. Then, the samples were roasted in a muffle furnace at 1230 °C for 1 h under air condition. Finally, chemical composition, XRD, and scanning electron microscopy (SEM)−EDS analyses were performed on the roasted samples.

4.2.2. Evaluated Methods of Deposit Adhesion on the Refractory Bricks. The initial stage of the deposit formation in rotary kilns is the adhesion process of the powder to the refractory bricks; the adhesion materials on the refractories provide the basis for the subsequent deposit growth. The experimental evaluation method used in this study was mentioned in our previous paper.[28] The simulated deposit samples (3 g) were placed uniformly on the surface of the refractory bricks (circular area of 3 cm in diameter) and roasted in a muffle furnace at 1230 °C for 5 h under an air atmosphere. As shown in Figure 11, after cooling, the samples were rolled by a roller with a certain mass twice to simulate the mechanical and impact actions from rolling pellets in the rotary kiln. Thus, the bonding degree between the deposits and the refractory brick by comparing proportions of the simulated deposit samples adheres to the refractory brick.

4.3. Analysis Methods. According to Chinese standards, the determination of the chemical composition of the raw materials is performed by chemical analysis methods.[28] Phase compositions of deposit samples with different binary basicity were analyzed by XRD (Empyrean, Malvern PANalytical, The Netherlands). The microstructure and phase composition of simulated experimental samples were determined using SEM (TESCAN, MIRA3-LMH, Czech) coupled with an energy-dispersive spectra analyzer (EDS, Oxford X-MAX20). FactSage8.0[32] software was used to calculate the liquidus temperatures and liquid amounts of the silicate phases as well as the phase diagram. Software uses the "Phase Diagram" and "Equilib" modules, as well as the corresponding "FactPS" and "FToxid" databases.

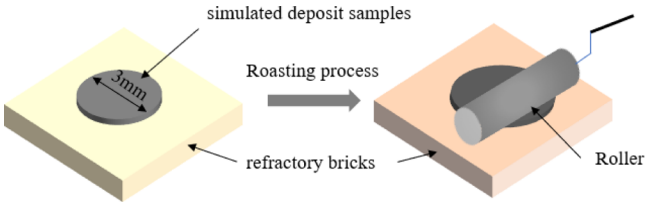

Figure 11. Schematic diagram of the evaluated method used in the present study.

AUTHOR INFORMATION

Corresponding Author

Shuai Wang − *School of Minerals Processing and Bioengineering, Central South University, Changsha, Hunan 410083, China;* orcid.org/0000-0002-5120-7752; Phone: +86-073188830346; Email: wang_shuai@csu.edu.cn

Authors

Yufeng Guo − *School of Minerals Processing and Bioengineering, Central South University, Changsha, Hunan 410083, China*

Zhuang Yang − *School of Minerals Processing and Bioengineering, Central South University, Changsha, Hunan 410083, China*

Jianjun Fan − *Technology Center, Taiyuan Iron Steel (Group) Co., Ltd (TISCO), Taiyuan, Shanxi 030003, China*

Feng Chen − *School of Minerals Processing and Bioengineering, Central South University, Changsha, Hunan 410083, China;* orcid.org/0000-0002-1977-6795

Lingzhi Yang − *School of Minerals Processing and Bioengineering, Central South University, Changsha, Hunan 410083, China*

Yajing Liu − *School of Minerals Processing and Bioengineering, Central South University, Changsha, Hunan 410083, China*

Kuo Liu − *School of Minerals Processing and Bioengineering, Central South University, Changsha, Hunan 410083, China*

Complete contact information is available at: https://pubs.acs.org/10.1021/acsomega.1c06800

Notes

The authors declare no competing financial interest.

ACKNOWLEDGMENTS

The authors would like to acknowledge the financial support from the National Natural Science Foundation of China (51904348), the Major Science and Technology Special Project of Shanxi Province (20191101002), and the Open Sharing Fund for the Large-scale Instruments and Equipments of Central South University (CSUZC202128).

https://doi.org/10.1021/acsomega.1c06800
ACS Omega 2022, 7, 4640−4647

REFERENCES

(1) Fu, J.; Jiang, T.; Zhu, D. *Sintering and pelletizing*; Central South University of Technology Press: Changsha, 1996.

(2) Kawatra, S. K.; Claremboux, V. Iron Ore Pelletization: Part I. Fundamentals. *Miner. Process. Extr. Metall. Rev.* **2021**, 1.

(3) Li, J.; An, H. F.; Liu, W. X.; Yang, A. M.; Chu, M. S. Effect of basicity on metallurgical properties of magnesium fluxed pellets. *J. Iron Steel Res. Int.* **2020**, *27*, 239−247.

(4) Prusti, P.; Barik, K.; Dash, N.; Biswal, S. K.; Meikap, B. C. Effect of limestone and dolomite flux on the quality of pellets using high LOI iron ore. *Powder Technol.* **2021**, *379*, 154−164.

(5) Wang, X.; Shi, X.; Hu, C.; Wang, X.; Hu, Q. Experimental study on sphericalation and cold performance of high-silica magnesium flux pellets. *J. Iron Steel Res.* **2020**, *32*, 212−219.

(6) Stjernberg, J.; Isaksson, O.; Ion, J. The grate-kiln induration machine — history, advantages, and drawbacks, and outl. *J. S. Afr. Inst. Min. Metall* **2015**, *115*, 137−144.

(7) Qiao, H.; Zhang, J.; Wang, Y.; Xu, C.; Liu, Z. Production practice and development trend of calcareous alkaline pellets around the world. *J. Iron Steel Res.* **2021**, *33*, 1031−1039.

(8) Ye, K. Review of three pellet roasting processes. *Sinter. and Pelletizing* **2002**, *1*, 4−7.

(9) Fan, X. H.; Yang, G. M.; Chen, X. L.; Gao, L.; Huang, X. X.; Li, X. Predictive models and operation guidance system for iron ore pellet induration in traveling grate−rotary kiln process. *Comput. Chem. Eng.* **2015**, *79*, 80−90.

(10) Stjernberg, J.; Ion, J. C.; Antti, M.-L.; Nordin, L.-O.; Lindblom, B.; Odén, M. Extended studies of degradation mechanisms in the refractory lining of a rotary kiln for iron ore pellet production. *J. Eur. Ceram. Soc.* **2012**, *32*, 1519−1528.

(11) Abouzeid, A.-Z. M.; Kotb, I. M.; Negm, A. A. Iron ore fluxed pellets and their physical properties. *Powder Technol.* **1985**, *42*, 225−230.

(12) Eriksson, M.; Carlborg, M.; Broström, M. Characterization of ring deposits inside a quicklime producing long rotary kiln. *Energy Fuels* **2019**, *33*, 11731−11740.

(13) Zhong, Q.; Yang, Y.; Jiang, T.; Li, Q.; Xu, B. Effect of coal ash on ring behavior of iron-ore pellet powder in kiln. *Powder Technol.* **2018**, *323*, 195−202.

(14) Fan, J.; Guo, Y.; Zang, L.; Wang, L. Effect of residual carbon in coal ash on formation of ring accretion of rotary pelletizing kiln. *China Metall* **2017**, *27*, 8−13.

(15) Jonsson, C. Y. C.; Stjernberg, J.; Wiinikka, H.; Lindblom, B.; Boström, D.; Öhman, M. Deposit formation in a grate-kiln plant for iron-ore pellet production. Part 1: characterization of process gas particles. *Energy Fuels* **2013**, *27*, 6159−6170.

(16) Stjernberg, J.; Jonsson, C. Y. C.; Wiinikka, H.; Lindblom, B.; Boström, D.; Öhman, M. Deposit formation in a grate-kiln plant for iron-ore pellet production. Part 2: characterization of deposits. *Energy Fuels* **2013**, *27*, 6171−6184.

(17) Wang, S.; Guo, Y.; Fan, J.; He, Y.; Jiang, T.; Chen, F.; Zheng, F.; Yang, L. Initial stage of deposit formation process in a coal fired grate-rotary kiln for iron ore pellet production. *Fuel Process. Technol.* **2018**, *175*, 54−63.

(18) Bandyopadhyay, R.; Gupta, S.; Lindblom, B.; Jonsson, S.; French, D.; Sahajwalla, V. Assessment of ash deposition tendency in a rotary kiln using Thermo-mechanical analysis and Experimental Combustion Furnace. *Fuel* **2014**, *135*, 301−307.

(19) Sefidari, H.; Ma, C.; Fredriksson, C.; Lindblom, B.; Wiinikka, H.; Nordin, L. O.; Wu, G.; Yazhenskikh, E.; Müller, M.; Öhman, M. The effect of co-firing coal and woody biomass upon the slagging/deposition tendency in iron-ore pelletizing grate-kiln plants. *Fuel Process. Technol.* **2020**, *199*, 106254.

(20) Kurose, R.; Ikeda, M.; Makino, H. Combustion characteristics of high ash coal in a pulverized coal combustion. *Fuel* **2001**, *80*, 1447−1455.

(21) Hamid, S.; Bo, L.; Henrik, W.; Lars-Olof, N.; Johanne, M.; Uddin, B. I.; Marcus, H. The effect of disintegrated iron-ore pellet dust on deposit formation in a pilot-scale pulverized coal combustion furnace. Part I: Characterization of process gas particles and deposits. *Fuel Process. Technol.* **2018**, *177*, 283−298.

(22) Fu, X.; Chen, Z.; Xu, X.; He, L.; Song, Y. Deposits in gas-fired rotary kiln for limonite magnetization-reduction roasting: characteristics and formation mechanism. *Metals* **2019**, *9*, 764.

(23) Jiang, T.; He, G.; Gan, M.; Li, G.; Fan, X.; Yuan, L. Forming mechanism of rings in rotary-kiln for oxidized pellet. *J. Iron Steel Res. Int.* **2009**, *16*, 292−297.

(24) Wang, S.; Guo, Y.; Fan, J.; Jiang, T.; Chen, F.; Zheng, F.; Yang, L. Deposits in a coal fired grate-kiln plant for hematite pellet production: Characterization and primary formation mechanisms. *Powder Technol.* **2018**, *333*, 122−137.

(25) Luo, G.; Nie, X.; Wu, S.; Wang, Y.; Liu, J.; Zhou, S. Influence of F, K, Na on the ring formation properties of oxidized pellet rotary kiln. *Sinter. Pelletizing* **2013**, *38*, 29−32.

(26) Fan, X.; Gan, M.; Yuan, L.; Li, G.; Jiang, T.; Zhuang, J. Study of mechanism on ring formation in grate-kiln of acid pellet. *Iron Steel* **2008**, *43*, 15−20.

(27) Guo, Y. F.; Wang, S.; He, Y.; Jiang, T.; Chen, F.; Zheng, F. Q. Deposit formation mechanisms in a pulverized coal fired grate for hematite pellet production. *Fuel Process. Technol.* **2017**, *161*, 33−40.

(28) Wang, S.; Guo, Y.-F.; Chen, F.; He, Y.; Jiang, T.; Zheng, F.-Q. Combustion reaction of pulverized coal on the deposit formation in the kiln for iron ore pellet production. *Energy Fuels* **2016**, *30*, 6123−6131.

(29) Zhang, Z.; Wu, X.; Zhou, T.; Chen, Y.; Hou, N.; Piao, G.; Kobayashi, N.; Itaya, Y.; Mori, S. The effect of iron-bearing mineral melting behavior on ash deposition during coal combustion. *Proc. Combust. Inst.* **2011**, *33*, 2853−2861.

(30) Fan, J.; Guo, Y.; Zang, L.; Shi, Y.; Li, H.; Zheng, F. Effect of basicity on properties of pellets produced by ultra fine-sized iron concentrate. *J. Iron Steel Res.* **2019**, *5*, 440−445.

(31) Wang, S.; Guo, Y.; Liu, K.; Yang, Z.; Liu, Y.; Jiang, Y.; Chen, F.; Zheng, F.; Yang, L. The deposit formation mechanism in coal-fired rotary kiln for iron ore pellet production: A review. *Crystals* **2021**, *11*, 974.

(32) Bale, C. W.; Bélisle, E.; Chartrand, P.; Decterov, S. A.; Eriksson, G.; Gheribi, A. E.; Hack, K.; Jung, I.-H.; Kang, Y.-B.; Melançon, J.; Pelton, A. D.; Petersen, S.; Robelin, C.; Sangster, J.; Spencer, P.; Van Ende, M.-A. FactSage thermochemical software and databases, 2010−2016. *Calphad* **2016**, *54*, 35−53.

https://doi.org/10.1021/acsomega.1c06800
ACS Omega 2022, 7, 4640−4647